Nanoscale

PAPER

View Article Online
View Journal | View Issue

Check for updates

Cite this: *Nanoscale*, 2025, **17**, 14193

Hydrogel–polymersome composites as a sensing platform for monitoring food spoilage†

Christoph John, Elena C. dos Santos, Riccardo Pascal Wehr, Daniel Messmer, Cornelia G. Palivan and Ionel Adrian Dinu *

The development of advanced functional soft materials for applications in preserving food quality and detecting spoilage is in focus today. While various smart food packaging options are available, there are still challenges to be addressed due to several limitations of current food quality sensors, such as a lack of multifunctionality, use of potentially harmful synthetic sensing molecules or short shelf life of natural analogues. Herein, we present a dual-functional hydrogel–polymersome composite (HPC) system that integrates two complementary sensing functionalities into a single platform. As a model for dual-functionality, we successfully incorporated dye-loaded polymersomes into a poly(*N*-isopropylacrylamide)-based hydrogel. This approach enables temperature-triggered cargo release, while the encapsulated dyes serve as pH-reporting molecules for monitoring food freshness. The first functionality was demonstrated by hydrogel shrinkage and subsequent release of dye upon increasing the temperature from 25 °C to 40 °C. The second functionality was probed by decreasing the pH to 6.2 or exposure to methylamine (MA), a representative volatile amine, which shifted the local pH to basic values. The HPCs remained stable under hydrated conditions, and their dual-functionality was proved using fluorescence spectroscopy and light scattering. Our system exhibited a detection limit of 1 mM MA—2.5 times lower than the threshold classified as acutely toxic by the Centers for Disease Control and Prevention—highlighting its relevance for spoilage detection. These findings demonstrate that combining functional polymersomes with stimuli-responsive hydrogels offers a promising approach for developing multifunctional, compartmentalized composite sensors suitable for integration into food packaging to efficiently monitor its freshness.

Received 8th December 2024,
Accepted 7th May 2025

DOI: 10.1039/d4nr05177g

rsc.li/nanoscale

Open Access Article. Published on 08 May 2025. Downloaded on 1/24/2026 9:10:55 AM.
This article is licensed under a Creative Commons Attribution-NonCommercial 3.0 Unported Licence.

Introduction

The increasing consumer demand for healthy, unprocessed, ready-to-eat or easy-to-prepare foods has become a major concern of our modern society as the globalization of food production and distribution has a great impact on the freshness and safety of food due to longer shipping times.[1] To suppress potential food spoilage and facilitate its detection, there is strong interest in developing smart materials that are specifically engineered to interact with packaged goods. Antimicrobial packaging represents one approach for eradicating or inhibiting the growth of pathogenic microorganisms, preventing spoilage and extending the shelf life of food.[2,3]

An appealing concept, complementary to preservation, is the monitoring and tracking of food spoilage since an increasing number of people are affected by food poisoning caused by bacteria, viruses, fungi and other contaminants, including traces of chemicals or natural toxins.[4] In this regard, intelligent packaging using smart strips or labels represents a next-generation technology that allows monitoring of the food status in real time and on-site. This approach not only informs the consumers whether the food is safe to eat, but also diminishes the need for expensive and time-consuming lab analyses to evaluate food quality.[5] Sensing platforms are also necessary to measure food freshness by indicating the temperature changes or the presence of volatile or biogenic amines resulting from food spoilage. For example, elevated temperature increases the microbiological activity in sealed packaged meat, where the increased CO_2 levels and the high moisture content lead to pH values below 7.0 and thereby to a decrease in freshness and spoilage.[1,6,7] A high level of total volatile basic nitrogen present in seafood indicates the formation of significant amounts of ammonia, dimethylamine and trimethylamine by the decomposition of

Department of Chemistry, University of Basel, Mattenstrasse 22, BPR 1096, CH-4002 Basel, Switzerland. E-mail: adrian.dinu@unibas.ch

†Electronic supplementary information (ESI) available: Additional information including DLS-SLS and NTA data, TEM micrographs, fluorescence emission spectra, CLSM and optical images are presented herein. See DOI: https://doi.org/10.1039/d4nr05177g

Open Access Article. Published on 08 May 2025. Downloaded on 1/24/2026 9:10:55 AM.
This article is licensed under a Creative Commons Attribution-NonCommercial 3.0 Unported Licence.

amino acids and other nitrogen-containing molecules and is associated with food poisoning.[8–14] The quantification of changes in the concentration of these toxic compounds would indicate the degree of spoilage and can be assessed accordingly by a sensing device.

An established tool to detect volatile or biogenic amines consists of pH-sensitive dyes embedded in a hydrophobic matrix.[15–17] However, the major drawbacks of such chemical sensors are their insufficient sensitivity, poor biocompatibility and safety issues caused by potentially toxic indicator molecules such as azo dyes embedded into the carrier polymer matrix.[18] To monitor food contamination, sensor units are immobilized onto a suitable support, such as indicator paper,[19,20] thin films,[21,22] polymer particles,[23,24] carbon nanotubes,[25] agarose hydrogels,[26] or porous silicone hydrogels embedding graphene oxide and gold nanoparticles.[27]

The design of "on-package" sensors, which are most commonly used to provide an overall estimation of food quality, is commonly based on pH-sensors.[28] Thus, pH-responsive dyes were immobilized onto a membrane filter paper to monitor the quality of beef over time[17] while a colorimetric sensor consisting of cellulose microparticles modified with pH-signalling dyes, embedded into a silicon matrix, has been developed to assess fish decomposition.[18] However, these sensors are so far only functional for a specific application field and are not designed to detect and respond to more than one type of trigger.[29,30] Therefore, it is still challenging to integrate different stimuli-reporting molecules into a single array or to combine spoilage detection with food preservation to achieve multifunctional sensing platforms.

Here we introduce a dual-reporting hydrogel–polymersome composite (HPC) system that integrates two complementary sensing functionalities into a single platform. This approach enables temperature-triggered cargo release, while the encapsulated dyes serve as pH-reporting molecules for monitoring food freshness. Such HPCs are suitable for the production of sensing strips that can be easily inserted into food packaging and provide information about food quality or preservation status. To this end, we encapsulated pH-reporting molecules in polymer nanocompartments, also known as polymersomes, which were then embedded in a temperature-responsive hydrogel. We selected polymersomes to encapsulate the reporting molecules due to their increased stability compared to liposomes[31–34] and their capacity for loading a large variety of molecules (enzymes,[35,36] drugs,[37,38] and contrast agents[39,40]).

The polymersomes were self-assembled from the amphiphilic diblock copolymer poly(dimethylsiloxane)-*block*-poly(2-methyl-2-oxazoline) (PDMS-*b*-PMOXA), already reported as forming polymer vesicles with a stable and flexible membrane[41] that are biocompatible and non-toxic.[42,43] Moreover, immobilized PDMS-*b*-PMOXA-based polymersomes served to produce "active" surfaces when loaded with sensitive dyes to detect small pH changes[5] or with different enzymes to support cascade reactions.[44] To increase the stability of polymersomes and introduce an additional response to stimuli, we chose to embed the polymersomes in the cross-linked matrix of a polymer hydrogel. Owing to their biocompatibility, tunable mechanical strength, and responsiveness to stimuli, hydrogels have been studied extensively for the controlled release of a broad variety of compounds.[45–47] However, there are only very few examples of HPCs,[48] mainly designed for medical applications, such as injectable hydrogels,[49–51] antifouling systems for therapeutic contact lenses,[52] or drug release systems.[51,53] HPCs have the advantages of allowing small molecules to

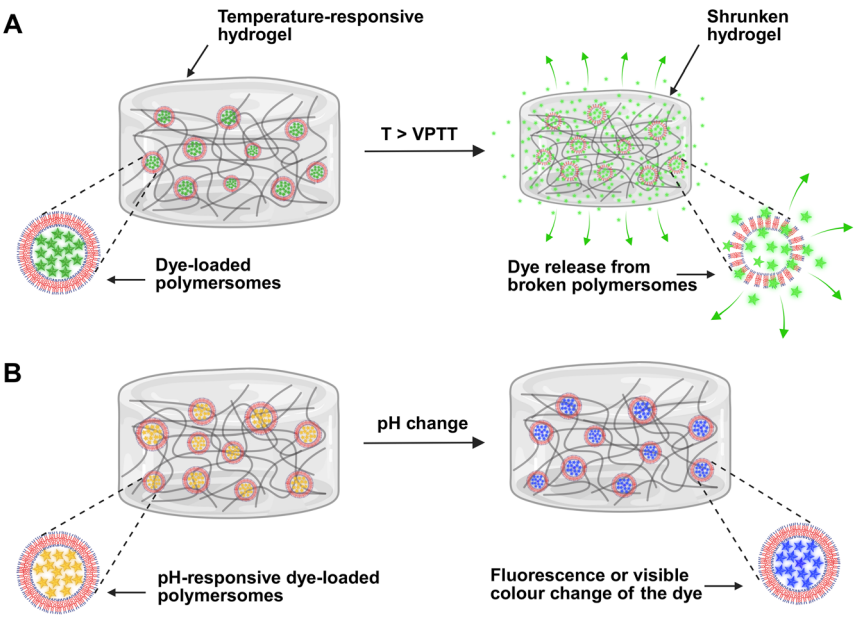

Fig. 1 Schematic illustrations of NIPAM-based hydrogels (HPCs) embedding dye-loaded polymersomes (A) after heating above the VPTT of PNIPAM, and (B) upon pH change of the outer environment. Created in BioRender. Kraus, M. (2025) https://BioRender.com/u06z774.

This journal is © The Royal Society of Chemistry 2025

Open Access Article. Published on 08 May 2025. Downloaded on 1/24/2026 9:10:55 AM.
This article is licensed under a Creative Commons Attribution-NonCommercial 3.0 Unported Licence.

diffuse throughout the hydrogel matrix and preventing the polymersomes from escaping the polymer network. Therefore, this combination brings considerable benefits in terms of stability, multifunctionality and biocompatibility. The selection of a poly(*N*-isopropyl acrylamide) (PNIPAM) hydrogel as a matrix for embedding polymersomes endows the HPCs with triggered release properties at temperatures above the volume phase transition temperature (VPTT) of the hydrogel (32–34 °C).[54] An increase in temperature above the VPTT induces shrinkage of the polymer network, which generates enough mechanical stress to disrupt the polymersome membrane, and thus release the reported molecules (Fig. 1).

To evaluate the stability of polymersomes inside the hydrogel network and assess the temperature-triggered release of the encapsulated cargo from polymersomes, we chose 5(6)-carboxyfluorescein (CF) as a model "reporter" compound. Pyranine (Py) and bromothymol blue (BTB) were used as responsive dyes to monitor the pH changes in the environment and the presence of amines (*i.e.* methylamine as a model representative) involved in food spoilage. By combining static and dynamic light scattering (SLS-DLS), nanoparticle tracking analysis (NTA) and transmission electron microscopy (TEM), we evaluated polymersome formation and assessed the integrity of the polymer membrane in the presence of pH-reporting molecules and the components involved in the synthesis of the PNIPAM hydrogel. The stimuli-responsiveness was evaluated by fluorescence measurements at various pH and temperature values. The change in colour at different pH values was also observed after a temperature-induced shrinkage, indicating that our composite responds to a combination of both stimuli. The temperature responsiveness triggers the release of an encapsulated molecule upon exposure to an external stimulus (inappropriate food temperature), which serves as a signal to identify the storage of food products under improper temperature conditions during their shelf life.

To our knowledge, there are no reports of dual-functional hydrogel–polymersome composites that successfully combine the use of pH-reporting molecules with the stimulus-triggered release of a cargo from polymersomes embedded in the hydrogel. The dual functionality of our system opens new perspectives for advances in sensors for food freshness monitoring.

Experimental

Materials

N-Isopropylacrylamide (NIPAM), poly(ethylene glycol) diacrylate (PEGDA) with a number-average molecular weight (M_n) of 575 g mol^{-1}, ammonium persulfate (APS), *N*,*N*,*N*′,*N*′-tetramethylethylenediamine (TEMED), 5(6)-carboxyfluorescein (CF), bromothymol blue (BTB), pyranine (Py), methylamine (MA), sodium dihydrogen phosphate anhydrous, disodium hydrogen phosphate dodecahydrate, Triton-X100 (Octoxinol 9) and *p*-xylene-bis(*N*-pyridinium bromide) (DPX) were purchased from Sigma Aldrich and used without further purification. Deionised water (Milli-Q water) was obtained using a MilliQ Q-POD device (Merck, Germany). The diblock copolymer $PDMS_{25}$-*b*-$PMOXA_{10}$ with M_n = 2850 g mol^{-1} and a dispersity ($Đ$) of 1.49 was previously synthesized in our group according to a reported protocol.[42]

Methods

Formation of polymersomes. Self-assembly of $PDMS_{25}$-*b*-$PMOXA_{10}$ diblock copolymers into polymersomes was performed by film rehydration. 5 mg of copolymer was first dissolved in 1.0 mL of ethanol in a 5 mL round-bottom flask. The solvent was then removed using a rotary evaporator at 40 °C, 40 rpm and 140 mbar for 2 h until the polymer film was completely dry. The dried polymer film was rehydrated with 1 mL Milli-Q water and stirred for 24 h at room temperature (RT) and 300 rpm. For the encapsulation of dyes, the polymer film was rehydrated with aqueous solutions of CF (100 μM or 50 mM, pH 8–9), Py (100 μM) or BTB (1.25 mM). To obtain polymersomes with a narrow size distribution, the dispersions of self-assemblies were extruded 13 times through Nucleopore Track-Etch membranes with a pore size of 200 nm (Whatman, USA) mounted on an Avanti Extruder (Avanti Polar Lipids, USA). The extruded dye-loaded polymersomes were purified by centrifugation through centrifugal filters (Amicon-Ultracel-30 K, Merck Millipore), which allow the separation of polymersomes from the free dye without diluting the sample. After 5 min of centrifugation at 13 400 rpm, the filtrate was removed and fresh Milli-Q water was added to the polymersome dispersion. The washing was repeated more than 10 times, until no dye was detected in the filtrate.

Preparation of hydrogels and hydrogel–polymersome composites. The reaction mixture used to prepare the hydrogel matrix was composed of 1 g NIPAM (8.85 mmol, 1 eq.), 51 mg PEGDA (88.1 μmol, 0.01 eq., M_n = 575 g mol^{-1}), and 10 mg APS (0.043 μmol, 0.005 eq.) dissolved in 5 mL of Milli-Q water. For the preparation of hydrogels and hydrogel–polymersome composites, 180 μL of the reaction mixture was mixed in 1 mL glass vials with either 180 μL of Milli-Q water or 180 μL of polymersome dispersion, respectively. The samples were bubbled with argon for 5 min, after which polymerization was activated by adding 1 μL of TEMED to the monomer mixtures. The vials were sealed with lids, and polymerization proceeded at room temperature for 24 h. Following polymerization, the resulting composite gels were immersed in excess Milli-Q water for one week to remove the unreacted components, changing the washing water every 24 h.

Characterization of swelling behaviour. The degree of swelling (DS) was determined gravimetrically in aqueous solution and calculated according to eqn (1):[55]

$$\mathrm{DS}\ [\%] = \frac{(m_f - m_i)}{m_i} \times 100 \quad (1)$$

where m_f – weight of hydrogel swollen in water at equilibrium [g] and m_i – weight of dry hydrogel [g].

To this end, dried hydrogels were placed in Milli-Q water at RT, and then swollen until the equilibrium was reached. The swollen samples were removed from water, carefully tapped

Open Access Article. Published on 08 May 2025. Downloaded on 1/24/2026 9:10:55 AM.
This article is licensed under a Creative Commons Attribution-NonCommercial 3.0 Unported Licence.

with a paper tissue to remove excess water, and then weighed. The swelling results were calculated as average values of triplicate measurements.

Dynamic and static light scattering (DLS-SLS). Light scattering data at different angles were obtained using a spectrometer (LS Instruments, Switzerland) equipped with a 633 nm He–Ne laser (21 mW). All experiments were measured at scattering angles between 30° and 135° at 25 °C in round-bottom glass cuvettes (10 × 0.9–1.0 mm, Boro 3.3). All samples were diluted to 0.05 mg mL^{-1} and measured without further filtration. Hydrodynamic radii (R_h) were calculated as mean values of three independent DLS measurements over the whole angle range using second-order cumulant analysis. The radii of gyration (R_g) were determined from SLS data using Mie scattering models (MiePlot, UK).[56] When there are insufficient scattering data to be evaluated by Mie fit, the Guinier plot was used to determine R_g from the measured scattered intensity as a function of the scattering vector q.

Transmission electron microscopy (TEM). TEM micrographs were recorded with a CM100 transmission electron microscope (Philips, Netherlands) at an acceleration voltage of 80 kV. Formvar-coated 200-mesh copper grids were glow-discharged for 30 s prior to use. Afterwards, 15 μL of the diluted self-assembly dispersion (0.5 mg mL^{-1}) was placed on the grid for adsorption and the excess was blotted off using filter paper after one minute. The grid was washed two times with 50 μL Milli-Q water and then 5 μL of a 2% aqueous uranyl acetate solution was added to the grid and blotted off immediately. Another 5 μL of uranyl acetate solution was placed on the grid for 10 s and blotted off before imaging.

Nanoparticle tracking analysis (NTA). NTA measurements were conducted with a NanoSight NS300 (Malvern Panalytical, UK) equipped with a 488 nm laser and then analysed using the NTA software (version 3.4). For the measurements, dilutions of 5–2.5 μg mL^{-1} polymer dispersions were prepared in Milli-Q water and the injection rate was set at 100 μL min^{-1}. The settings for the camera level were chosen to track 30–50 particles per frame. Five repetitions of 60 s each were recorded, and then the hydrodynamic diameters and size distribution of polymersomes were calculated based on the Einstein–Stokes equation and averaged over all measurements.

Preparation of the phosphate buffer. 10 mM phosphate buffer solutions with various pH values were prepared by dissolving 1.20 g (0.01 mol) anhydrous sodium dihydrogen phosphate in Milli-Q water and diluting the solution to 1000 mL. The pH of each solution was then adjusted to the appropriate pH value (pH 6.2, 6.5, 7.0, 7.5, and 8.0) by adding under stirring a solution of disodium hydrogen phosphate dodecahydrate (10 mM, 3.58 g L^{-1}) while monitoring the pH with a calibrated pH meter.

Fluorescence measurements. Fluorescence measurements were recorded with an FP-8200 fluorescence spectrometer (Jasco, Japan). All liquid samples (solutions of free dyes and dispersions of dye-loaded polymersomes) were measured in quartz cuvettes of 3.5 mL volume and 10 mm path length. The fluorescence of swollen HPCs was measured in their hydrated form using a standard set-up for measuring fluorescence on surfaces, *i.e.* placing them between two glass slides mounted into a specialized sample holder. To evaluate whether the polymersome integrity is preserved during hydrogel synthesis, a Triton-X100 solution (0.05%, v/v, in the final mixture) was added to disrupt the membrane of CF-loaded polymersomes (CF-P), and the fluorescence of CF was measured before and after the addition of the surfactant. Fluorescence excitation spectra of Py were recorded within an excitation wavelength range of 300 to 500 nm and emission at 511 nm. Py was either free in solution, encapsulated in polymersomes, or encapsulated in polymersomes embedded in a NIPAM-based hydrogel. For the quenching of free Py, the *p*-xylene-bis(*N*-pyridinium bromide) (DPX) quencher was used in excess at concentrations of 1.6 mM or 5.0 mM.

UV–Vis measurements. UV–Vis absorption measurements were recorded with a Cary 300 UV-Vis spectrometer (Agilent, USA). All samples were measured in a rectangular micro-quartz cell of 80 μL volume and 10 mm path length. Samples of BTB in 10 mM phosphate buffer with various pH values (pH 6.2–8.0) were prepared by mixing 10 μL of the aqueous BTB solution (50 μM) with 90 μL of the corresponding phosphate buffer. Mixtures of BTB and MA were prepared by mixing 10 μL of BTB (50 μM) with 90 μL of the MA solution (1 μM–10 mM). Dispersions of BTB-Ps in the presence of different concentrations of MA (1 μM–10 mM) were prepared by adding 10 μL of the dispersion of BTB-Ps to 90 μL of the respective MA solution.

Confocal laser scanning microscopy (CLSM). A Zeiss Axio Observer inverted microscope with an LSM 880 laser scanning unit (Carl Zeiss, Germany) equipped with an oil immersion objective (Plan-Apochromat 63×/1.4 Oil DIC M27) was used to perform CLSM measurements at 25 °C. The samples containing CF were excited with a 488 nm argon laser, collecting the fluorescence in the range of 518–600 nm. Each sample was unidirectionally scanned using 2048 × 2048 pixels with a bit depth of 16 bit. Images were processed using ImageJ (1.53c) and Zen Blue software (v. 3.2, Carl Zeiss, Germany).

For time-lapse fluorescence measurements upon the addition of Triton X-100 (20 μL of the surfactant solution, 0.05%, v/v), fluorescence images of an HPC slice of approximately 1 mm thickness were captured every 10 s in a 10 min time interval. The fluorescence values represent the mean fluorescence intensity from the 'green' channel.

Results and discussion

To generate multifunctional HPCs by the entrapment of polymersomes into the cross-linked matrix of a PNIPAM hydrogel, we first prepared polymersomes containing pH-sensitive molecules. We selected $PDMS_{25}$-*b*-$PMOXA_{10}$ as the amphiphilic diblock copolymer that was previously shown to form stable polymersomes in aqueous media.[42]

Formation and characterization of dye-loaded polymersomes

Polymersomes were formed *via* film-rehydration and loaded with reporting hydrophilic molecules. To efficiently respond to

 This journal is © The Royal Society of Chemistry 2025

Open Access Article. Published on 08 May 2025. Downloaded on 1/24/2026 9:10:55 AM.
This article is licensed under a Creative Commons Attribution-NonCommercial 3.0 Unported Licence.

food-relevant temperature and pH changes, we chose to separately encapsulate three different dyes, each serving a specific purpose. CF was used as a fluorescent model compound to evaluate the stability of polymersomes when entrapped within the hydrogel matrix and indicate the temperature-sensitive release from HPCs. Py, a fluorescent dye with a high sensitivity towards pH changes (pH ranging from 6.0 to 9.0) was selected to evaluate the overall pH sensitivity of HPCs and the stability of polymersomes within the polymer network. BTB was used to integrate a visible, pH-dependent colour change as a response to the presence of amines.

Light scattering (DLS-SLS) was used first to determine the architecture of the assemblies generated by the $PDMS_{25}$-*b*-$PMOXA_{10}$ copolymers without and with encapsulated dyes (Table 1 and Fig. S1 to S4, ESI†). The empty polymersomes had an average R_h of 107 ± 10 nm, whereas their R_g was 120 ± 6 nm, (Table 1 and Fig. S1, ESI†). The shape factor ρ of 1.12 ± 0.12, which is close to 1.0 (Table 1), is characteristic of hollow spheres with thin membranes.[31] The NTA measurements established an average R_h value of 93 ± 26 nm (Fig. S5, ESI†), which agrees with the light scattering results. In addition, the typical spherical deflated morphology of the empty polymersomes was observed by TEM (Fig. S6, ESI†).

The dye-loaded polymersomes after purification were analysed in a similar manner to evaluate the effect of dye encapsulation. Neither the light scattering data nor the NTA analysis indicates any significant changes in the size or aggregation of the polymersomes once loaded with reporting molecules (Table 1, Fig. S2 to S4 and S7, ESI†). The slightly smaller values of R_h obtained in all cases from NTA compared to DLS are due to the methodological differences between these two methods: DLS is generally biased towards bigger particles, particularly for polydisperse samples, resulting in higher average R_h values. TEM micrographs of the reporting molecules-loaded polymersomes reveal the presence of polymersomes (Fig. 2A and Fig. S8, ESI†).

The formation of HPCs requires polymersomes to remain stable when the PNIPAM hydrogel is formed. Therefore, polymersomes were also characterized in the presence of either the reaction mixture (NIPAM, PEGDA, and APS) or the solution of the activating agent (TEMED) (Table 1, Fig. S9 and S10, ESI†). The R_h and R_g values of polymersomes in the reaction mixture (103 ± 10 nm; 112 ± 6 nm) as well as in the aqueous TEMED solution (100 ± 6 nm; 105 ± 5 nm) clearly demonstrate that there are no changes in the polymersome integrity or aggregation following the exposure to reaction conditions specific to hydrogel synthesis.

Synthesis and temperature-dependent behaviour of PNIPAM-based hydrogels

The PNIPAM matrix was synthesized in the presence of various amounts of the PEGDA cross-linker. To find the optimal balance between the hydrogel integrity and its ability to shrink at temperatures above the VPTT, swelling tests were performed and the degree of swelling (DS, %) was determined gravimetrically (Fig. 2B).

When the swelling experiments were conducted at 25 °C, the DS values decreased on increasing the cross-linker content, as expected. At 0.5 mol% PEGDA cross-linker, the DS value was higher than 4500%, then decreased to 2300% for 1 mol% and 1000% for 10 mol% cross-linker content, respectively. In contrast, at 40 °C, the DS values are by a factor of 10 to 50 times smaller, showing a less significant cross-linker dependency (Fig. 2B). This trend can be attributed to the VPTT behaviour of PNIPAM polymer chains (32–34 °C).[54] At temperatures above this critical value, the hydrophobic interactions between the polymer chains are favoured, whereas the hydrogen bonding is weakened, leading to an extensive shrinkage of PNIPAM-based hydrogels and, generally, to less swelling. As a result, the hydrogel swelling at 40 °C is not dependent on the cross-linking degree, even though the use of PEGDA as a hydrophilic cross-linker might counterbalance the VPTT behaviour to a certain extent.[54,57] A considerable difference between the swollen states of PNIPAM hydrogels at various temperatures is required to significantly increase the potential of releasing any encapsulated cargo from the hydrogel upon the increase in temperature. The hydrogels with 1 mol% cross-linker, showing a 50-fold difference between the DS values at RT and at 40 °C, exhibited a pronounced thermo-responsive behaviour and relatively soft mechanical properties. As a consequence, this hydrogel composition was further used in preparing all HPCs reported in this study.

These hydrogels have a characteristic porous structure (Fig. 2C and D), with pore sizes in the range of several micro-

Table 1 DLS-SLS and NTA data for the $PDMS_{25}$-*b*-$PMOXA_{10}$ self-assembled polymersomes without or with encapsulated dyes, in the presence of the reaction mixture or TEMED

	DLS and SLS				NTA
Polymersomes	R_h [a] (nm)	R_g [b] (nm)	$\rho = R_g/R_h$	PDI	R_h (nm)
Empty polymersomes (Ps)	107 ± 10	120 ± 6	1.12 ± 0.12	0.19	93 ± 26
CF-loaded polymersomes (CF-Ps)	103 ± 11	115 ± 6	1.12 ± 0.13	0.23	90 ± 24
Py-loaded polymersomes (Py-Ps)	106 ± 14	120 ± 6	1.13 ± 0.16	0.20	77 ± 21
BTB-loaded polymersomes (BTB-Ps)	85 ± 6	96 ± 5	1.13 ± 0.10	0.20	79 ± 16
Empty polymersomes in the reaction mixture	103 ± 10	112 ± 6	1.09 ± 0.12	0.22	—
Empty polymersomes in TEMED solution	100 ± 6	105 ± 5	1.05 ± 0.08	0.19	—

[a] Derived from DLS. [b] Determined from SLS.

Open Access Article. Published on 08 May 2025. Downloaded on 1/24/2026 9:10:55 AM.
This article is licensed under a Creative Commons Attribution-NonCommercial 3.0 Unported Licence.

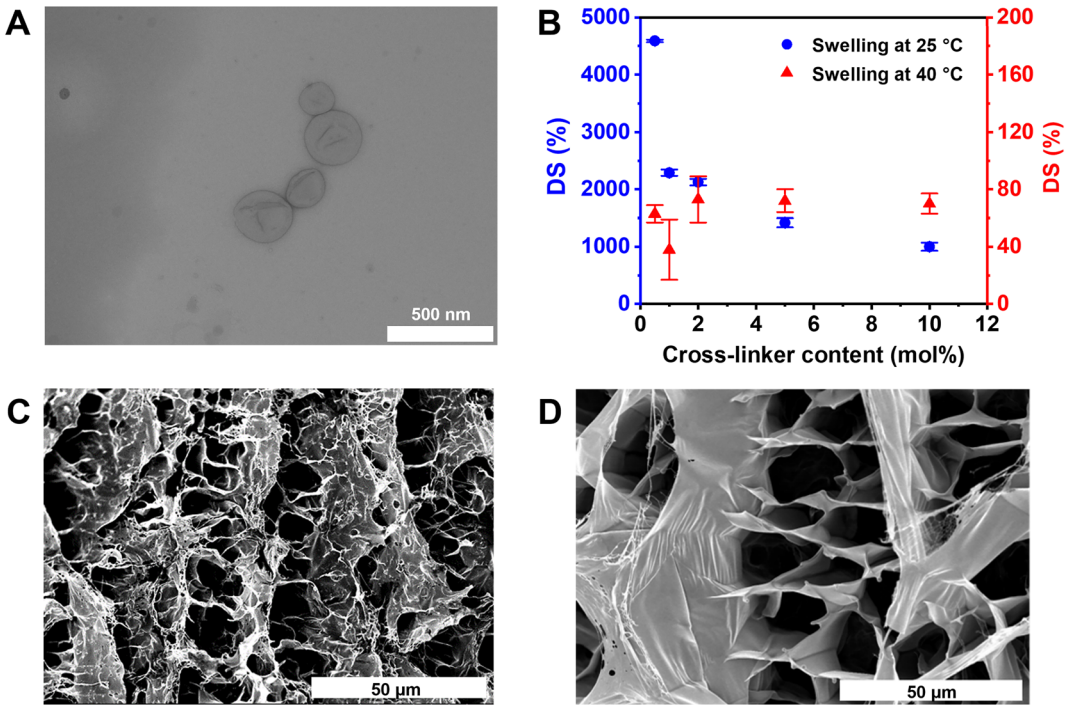

Fig. 2 Characterization of polymersomes. TEM micrograph of CF-loaded $PDMS_{25}$-*b*-$PMOXA_{10}$ polymersomes (CF-Ps, scale bar: 500 nm) (A); characterization of hydrogels and HPCs (B–D). Degree of swelling (DS) for PNIPAM-based hydrogels cross-linked with various amounts of PEGDA at temperatures below and above the LCST (B); SEM micrograph of a lyophilized PNIPAM-based hydrogel with a content of 1 mol% cross-linker (scale bar: 50 μm) (C); SEM micrograph of a lyophilized PNIPAM-based hydrogel, with a content of 1 mol% cross-linker and polymersomes incorporated (scale bar: 50 μm) (D).

metres, big enough to accommodate polymersomes of the sizes presented above.

Embedding polymersomes in PNIPAM hydrogels

For further analysis, it is important to guarantee that the process of embedding the polymersomes into the hydrogel matrix is not by itself harmful to the polymersome integrity. We used the addition of the surfactant Triton-X100, which is known to disrupt the polymersome membrane,[58] as a reference method to completely rupture the polymersomes embedded in the hydrogel. To evaluate the stability of polymersomes in the presence of a surfactant, the fluorescence of aqueous dispersions of CF-loaded polymersomes (CF-Ps), with CF encapsulated at a self-quenching concentration (20 mM), was measured before and after the addition of Triton-X100 (Fig. S11, ESI†). The increase in the fluorescence intensity of CF by approximately three times after the addition of the surfactant (0.05%, v/v, in the final mixture) indicates the rupture of the polymersome membrane, leading to dilution of the previously-encapsulated CF. To prepare HPCs with physically entrapped polymersomes, PNIPAM hydrogels with the 1 mol% PEGDA cross-linker were synthesized in the presence of dye-loaded polymersomes. The hydrogel composites entrapping CF-loaded polymersomes (CF-Ps) are referred to as CF-HPCs. The stability of CF-Ps entrapped in the hydrogel matrix was assessed first by evaluating the concentration of CF extracted from these composite hydrogels upon washing with excess water and compared with that extracted from hydrogels loaded with free CF only. For reasons of comparability, we used CF-loaded polymersomes (CF-Ps) without purification from excess free dye to maintain identical starting dye concentrations for the hydrogels. In this way, both hydrogels had initially the same amount of dye (100 μM CF) entrapped in their polymer matrix (Fig. 3A). While this approach provided comparable initial conditions, it resulted in close CF-release profiles for both the free CF-containing hydrogel and the HPC-containing CF-Ps and free CF, reaching a plateau after about 50 h. Even though this approach makes the effect of encapsulation less visible, a consistent 10–15% lower cumulative fluorescence intensity was observed in the supernatant after washing the HPC compared to the free CF-containing hydrogel during the final stage of extraction. This difference indicates that a fraction of the dye remained encapsulated within polymersomes and did not leak out over time.

After reaching the plateau in cumulative fluorescence intensity, the subsequent addition of Triton X-100 resulted in further dye release from the HPCs, indicating the stability of polymersomes and the presence of encapsulated CF that leaks out only after the disruption of the polymersome membrane (Fig. 3A). In addition, it is important to note that the overall increase in fluorescence would remain limited, as the penetration of Triton X-100 through the PNIPAM-based composite

 This journal is © The Royal Society of Chemistry 2025

Open Access Article. Published on 08 May 2025. Downloaded on 1/24/2026 9:10:55 AM.
This article is licensed under a Creative Commons Attribution-NonCommercial 3.0 Unported Licence.

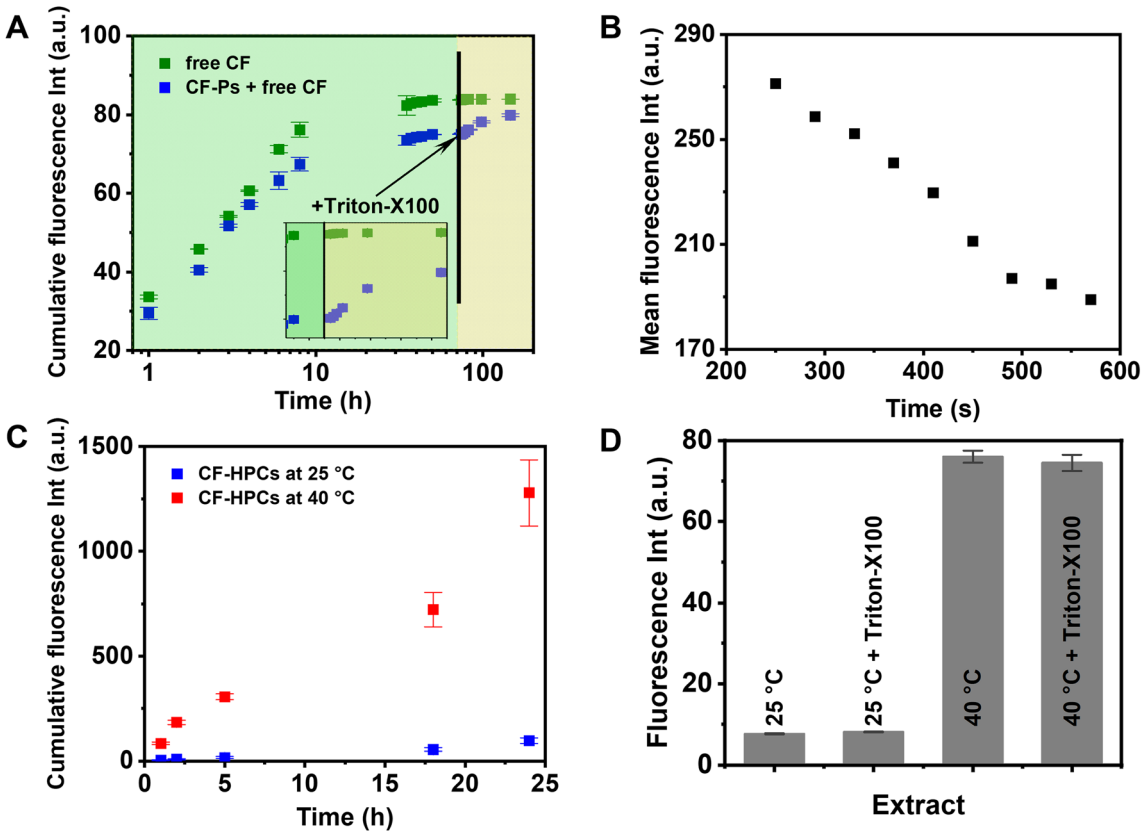

Fig. 3 Release profiles of the free dye (CF) from hydrogels and HPCs embedding CF-loaded polymersomes and free CF (CF-Ps + free CF) at RT. The inset represents a section from the dye release kinetics showing the changes in cumulative fluorescence upon the addition of Triton-X100 (A). Cumulative fluorescence extracted from the CLSM time-lapse micrographs of a slice of CF-HPC at 25 °C upon the addition of surfactant. The decrease in fluorescence intensity over time indicates the loss of the dye due to the rupture of the polymersome membrane (B). Dye release profile from CF-HPCs at 25 °C (blue squares) and 40 °C (red squares), respectively (C). Fluorescence intensity of the aqueous phase collected after 24 h washing of CF-HPCs at 25 °C and 40 °C. The fluorescence intensity (excitation at 495 nm, emission at 517 nm) was also measured before and after the addition of Triton-X100 to the collected aqueous phase. The lack of change in fluorescence intensity after the addition of surfactant indicates that no polymersome leaked out of the hydrogel (D).

matrix is a slow, diffusion-controlled process. Consequently, only a small fraction of polymersomes would be reached and eventually disrupted once the surfactant molecules enter the hydrogel and interact with the vesicle membrane. To complement the analysis of polymersome stability in the HPCs, we used CLSM. A slice of approximately 1 mm in thickness was cut from the HPC and washed out to remove the free dye. A series of CLSM micrographs was recorded (Fig. S12, ESI†) and the change in fluorescence after the addition of Triton-X100 was recorded over time (Fig. 3B). In the CLSM micrographs, the green fluorescence of encapsulated CF is localized and corresponds to the polymersomes distributed within the hydrogel. A time-lapse of CF-HPC showed that the fluorescence originating from the encapsulated CF decreased from the outside to the inside of the hydrogel within about 500 s after the addition of Triton-X100 (0.05%, v/v) due to the diffusion of dye out of the ruptured polymersomes (Fig. S12, ESI†). Both fluorescence spectroscopy and CLSM indicate that polymersomes preserve their morphology by entrapment into a hydrogel network.

CF-loaded HPCs as temperature-responsive platforms

We used a PNIPAM-based hydrogel as a temperature-sensitive polymer matrix because it shrinks at temperatures above its VPTT.

Thus, this allows to study whether it is possible to release the encapsulated cargo upon breaking the polymersomes *via* the mechanical stress generated by hydrogel shrinkage. CF was used as the entrapped model compound to evaluate the responsiveness of HPCs upon the temperature increase from 25 °C to 40 °C. First, the stability of polymersomes at the selected temperatures was evaluated by measuring the fluorescence intensity of the dispersions of CF-Ps after their storage for 24 h at 25 °C or 40 °C, respectively (Fig. S11, ESI†). No significant changes in fluorescence were observed for polymersomes stored at these temperatures. The increase in fluorescence after the addition of Triton-X100 (0.05%, v/v, in the final mixture) originates from the dilution of CF encapsulated in polymersomes at the self-quenching concentration, indicating that CF-Ps were stable at 40 °C. In a second step, HPCs

Open Access Article. Published on 08 May 2025. Downloaded on 1/24/2026 9:10:55 AM.
This article is licensed under a Creative Commons Attribution-NonCommercial 3.0 Unported Licence.

were stored under the same conditions in Milli-Q water and the fluorescence of the collected aqueous phase was measured over time. When the HPC was stored at 25 °C, only a minor change in fluorescence intensity was detected over 24 h (Fig. 3C). However, this minor increase is not an indication of significant dye leakage induced by the mechanical instability of polymersomes. We consider this dye release to be influenced by the mechanical deformation of HPCs during handling—such as during the repeated removal and replacement of washing solutions—and which can induce shear stress on the soft composite matrix. This stress may determine the rupture of a small fraction of embedded polymersomes, leading to the release of a minor fraction of the encapsulated dye. These effects are localized and do not reflect a general loss of polymersome integrity, consistent with the high stability reported for PDMS-*b*-PMOXA polymersome systems.[59–61] These polymer nanocompartments exhibit high colloidal stability, retaining their structural and functional integrity over extended periods of time—up to six months—when stored at 4 °C or 37 °C, without significant cargo leakage.[60,61] In contrast, the CF release observed in Fig. 3C upon heating (40 °C) is governed by the rapid volume phase transition of the hydrogel above its VPTT. The shrinkage of the whole hydrogel network generates sufficient mechanical stress to rupture the membrane of a significant number of polymersomes. This results in a tenfold increase in fluorescence, indicating a more pronounced release of the encapsulated reporting molecules (Fig. 3C). A quantitative analysis of DLS scattering data of the aqueous phase collected over time from the CF-HPCs stored at 40 °C was not possible, due to the very low scattering count rate. However, such a low count rate indicates the absence of self-assembled nanostructures, *i.e.* polymersomes. In addition, the fluorescence intensity of the aqueous phase did not change after the addition of Triton-X100, which also confirms that no polymersomes were released from the matrix during the hydrogel collapse (Fig. 3D). The shrinkage of hydrogels entrapping functional polymersomes is a promising strategy for inducing triggered release of an encapsulated cargo upon exposure to an adequate external stimulus. If the release is used to distribute and spread a compound that can be easily detected, such as a fluorescent dye, it can successfully be used as a temperature sensor in freight to indicate whether inappropriate temperature conditions were reached.

Py-loaded HPCs as pH-responsive sensing devices

Py is a water-soluble pH-reporting fluorescent dye with an emission maximum at 511 nm (λ_{ex} = 460 nm at pH ≈ 7). The fluorescence of Py decreases below pH 7 and increases above this value. The particular response around pH 7 renders Py very interesting not only for sensing the intracellular pH,[62] but also for detecting the small pH changes occurring in food products as a result of degradation. In a previous study, polymersomes encapsulating Py, which were immobilized on a solid surface, were able to detect and respond to the pH of the outer environment.[5] To prepare HPC sensors with a high sensitivity towards pH changes, we encapsulated Py in polymersomes (Py-Ps), which were subsequently entrapped into the PNIPAM hydrogel (Py-HPC). The pH-dependent fluorescence intensities of free Py, Py-Ps, and Py-HPCs were evaluated to establish the specific response towards pH changes (Fig. 4). By decreasing the pH to 6.2, a decrease of fluorescence intensity at 511 nm was observed for free Py (Fig. 4A).

The excitation spectra of Py-Ps aqueous dispersions, which were purified from the excess of free dye, reveal a similar pH

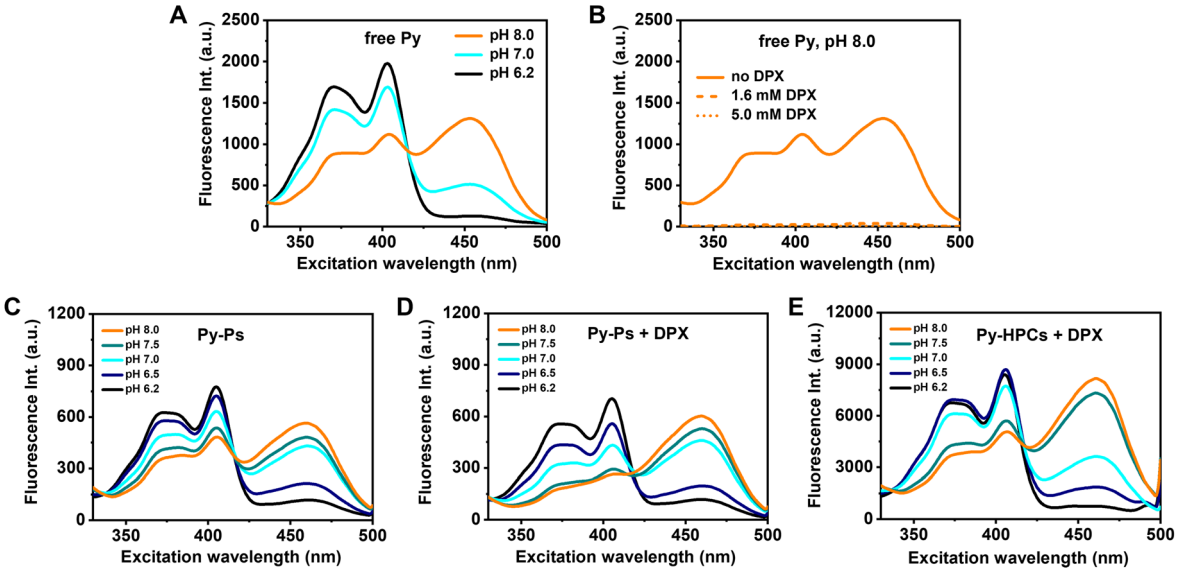

Fig. 4 Fluorescence excitation spectra of free Py in aqueous solutions with various pH values (emission wavelength 511 nm) (A); free Py in aqueous solutions with DPX as the quenching agent, at pH 8 (B); aqueous dispersions of Py-Ps at various pH values in the absence (C) and the presence of DPX (D); Py-HPCs measured in their hydrated and swollen form when placed between two glass slides and mounted into a specialized sample holder, in the presence of DPX at various pH values (E).

This journal is © The Royal Society of Chemistry 2025

Open Access Article. Published on 08 May 2025. Downloaded on 1/24/2026 9:10:55 AM. This article is licensed under a Creative Commons Attribution-NonCommercial 3.0 Unported Licence.

dependence as the free dye, with the fluorescence intensity decreasing from pH 8.0 to 6.2 (Fig. 4C). To exclude potential residual fluorescence originating from traces of free dye, a cationic quenching agent, DPX, was added in excess. This ensures that all free dye is fully quenched, whereas the dye encapsulated in the polymersomes remains protected from DPX and thus retains its fluorescence. The influence of the quencher on the fluorescence of Py was evaluated on solutions of free Py (Fig. 4B), dispersions of Py-Ps (Fig. 4D), and swollen Py-HPCs (Fig. 4E). As the fluorescence spectra showed no quenching effect of DPX on the encapsulated Py, the change in fluorescence measured on the surface of Py-HPCs indicates the successful response of our HPCs to pH changes in the external environment. The decrease in fluorescence is the strongest between pH 7 and pH 6.5, thus making the Py-Ps and Py-HPCs more sensitive to changes occurring in this pH range. Therefore, the Py-based systems would be highly sensitive to food that undergoes slight acidification during spoilage.

BTB-loaded HPCs as optical sensors for the detection of volatile amines

To facilitate the detection of food quality without the need for specialized analytical equipment that detects fluorescence, the HPCs were modified to provide a visible response. As volatile amines produced by microorganisms represent a major indicator of food spoilage, we specifically selected methylamine (MA) as a model amine. MA was mainly chosen due to its easy availability, relatively high vapour pressure compared to amines with longer carbon chains, and its strong ability to shift the local pH toward basic values. In addition, considering the potential health risks associated with MA at ingested concentrations higher than 2.5 mM,[63,64] we investigated concentrations ranging from 1 μM to 12 mM which include this critical level. Although amines with more carbon atoms commonly appear during food spoilage, MA serves as a model compound to validate the underlying sensing mechanism.

We selected BTB as a pH-reporting dye, which has a pk_a of 7.4 and changes its colour from yellow over green to blue when the pH shifts from acidic to basic.[65] BTB was encapsulated in polymersomes (BTB-Ps), which were entrapped into the hydrogel network (BTB-HPC). Then, we evaluated the pH-dependent absorbance of free BTB (Fig. 5A) and the potential of BTB-Ps to detect the presence of volatile amines that can turn the pH of food to slightly basic (Fig. 5C and Fig. S13B, ESI†). An increase in colour intensity was evident for free BTB when MA concentration increased from 0.12 mM to 12 mM (Fig. S13A, ESI†). The dye encapsulated in BTB-Ps revealed a similar concentration dependence, since a transition from yellow to blue was observed when MA concentration was increased in the same concentration range (Fig. S13B, ESI†). The strongest shift in BTB absorbance was observed between 100 μM and 1 mM of MA (Fig. 5B and C), which makes the concentration of 1 mM the lowest limit for visual detection of MA. By increasing the amine concentration, a colour shift to darker blue was visible with the naked eye. This colour shift is correlated with the protonation equilibrium of BTB. For free BTB in aqueous solution, the maximum absorption was reached at 1 mM MA and did not change with further increase of amine concentration (Fig. 5B), indicating that the equilibrium was completely shifted towards the deprotonated form. We then tested the response of the dispersions of BTB-Ps to various concentrations of MA (Fig. 5C).

The dispersions of BTB-Ps showed a similar limit for the visual detection of MA (about 1 mM), but a slightly different behaviour was observed when the concentration was varied from 1 mM to 10 mM, where a further increase in absorption was visible for BTB-Ps but not for free BTB. This particular difference can be associated with the hindered access of amine molecules or hydroxide ions to the encapsulated BTB molecules. This is dependent on the diffusion of hydroxide ions or protonated amines through the hydrophobic PDMS domain of the polymersome membrane. To prepare HPCs sensing the presence of MA, we entrapped the BTB-Ps into the hydrogel during its synthesis. BTB-HPCs behaved in a similar manner, changing their colour in the presence of MA, which makes our composites promising in the detection of food spoilage. It should be noted that while our hydrogel-based sensor does not specifically differentiate between different amines, it reliably detects local pH changes caused by the dissolution of amine vapours in the aqueous environment of the hydrogel and protonation. The subsequent protonation equilibrium generates hydroxide ions, which diffuse through the polymer-

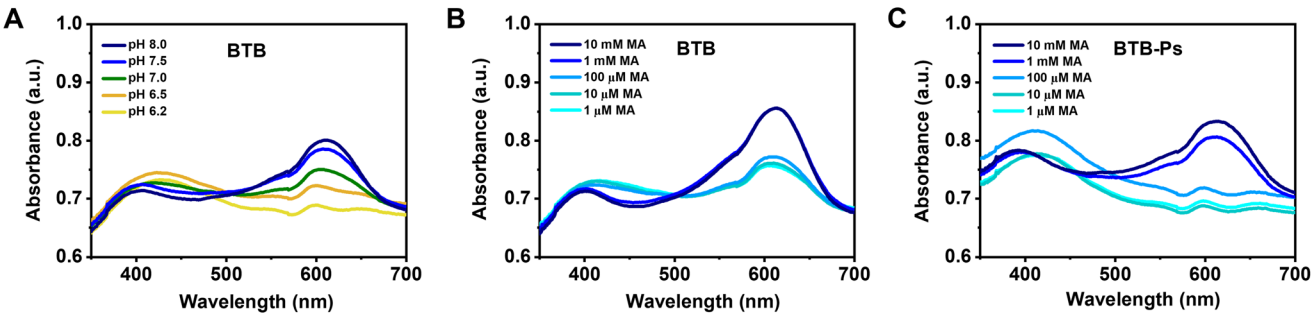

Fig. 5 UV-Vis absorption spectra of free BTB (5 μM) in 10 mM phosphate buffer of different pH values (pH 6.2–8.0) (A) and at various concentrations of MA (1 μM–10 mM) (B); UV-Vis absorption spectra of dispersions of BTB-Ps in the presence of various concentrations of MA (1 μM–10 mM) (C).

Open Access Article. Published on 08 May 2025. Downloaded on 1/24/2026 9:10:55 AM.
This article is licensed under a Creative Commons Attribution-NonCommercial 3.0 Unported Licence.

some membrane, interacting with the encapsulated pH-signalling molecules to trigger a visible response. Future studies will extend the evaluation of these sensors towards other spoilage-associated amines.

Dual functionality of reporting molecule-loaded HPCs

The contact between the sensor and analyte can be achieved with either the liquid phase containing the analyte or its vapours if the analyte is sufficiently volatile. The sensitivity of BTB-HPCs towards the presence of volatile amines was further evaluated using a set-up where no direct contact between methylamine and the sensing HPCs was allowed (Fig. 6). A small piece of wet pH-indicator paper was also placed into the glass chamber as a reference for reporting the pH changes in solution due to the presence of the amine. As expected, the pH-indicator paper started to change its colour already after 5 min of exposure and became completely blue after 1 h. The BTB-HPCs needed a longer time to shift their colour, a slight change from yellow to green occurring after about 1 h, whereas after 3 h a darker green-blue colour was clearly visible.

Since BTB-HPCs do not respond specifically to amine itself but rather detect local pH changes arising from amine dissolution and subsequent protonation, their response to MA is controlled by the diffusion of amine molecules through the hydrogel matrix and the transport across the polymersome membrane; therefore, a slower response is expected for the BTB-HPCs compared to the pH-indicator paper. The slightly delayed response when using BTB-HPCs has the advantage of preventing the leakage of the encapsulated dye, while the pH paper already lost some of its dye after 5 min of contact with the liquid. Thus, any variation in the environmental pH—whether acidic or basic—will influence the sensor response. Therefore, our BTB-HPC system provides a general pH-based signal rather than an amine-specific response. A further benefit of using BTB-HPCs over the pH-indicator paper was evident when the set-up was left in the open air for 5 days, until complete drying. The pH-indicator paper lost its colour, whereas the HPC maintained its light green colour even after drying (Fig. S14, ESI†).

This indicates that the hydrogel network entrapping BTB-loaded polymersomes experiences a lower rate of water loss during drying and thus allows for the preservation of BTB functionality. Therefore, the simple contact of BTB-HPCs with amine vapours is enough to generate an optical signal when amines are formed as a result of food degradation.

To assess whether the pH-sensing capability of BTB-HPC remains unaffected after exposure to elevated temperatures and to evaluate the potential leakage of reporting molecules due to hydrogel shrinkage, a BTB-HPC was heated in water at 40 °C for 2 h. Then, its ability to detect MA was investigated (Fig. S14, ESI†). This was again performed using the set-up presented in Fig. 6, and the heated BTB-HPC showed a colour response in the presence of MA vapours. A clear change in colour became visible after 3 h, which is still within a reasonable time frame. In this way, the HPCs can function as a platform to provide both temperature-induced dye release and pH-dependent response in the form of fluorescence or a signal visible with the naked eye. Despite their softness, the hydrogel–polymersome composites (HPCs) exhibit good mechanical stability when fully hydrated, with their dual functionality

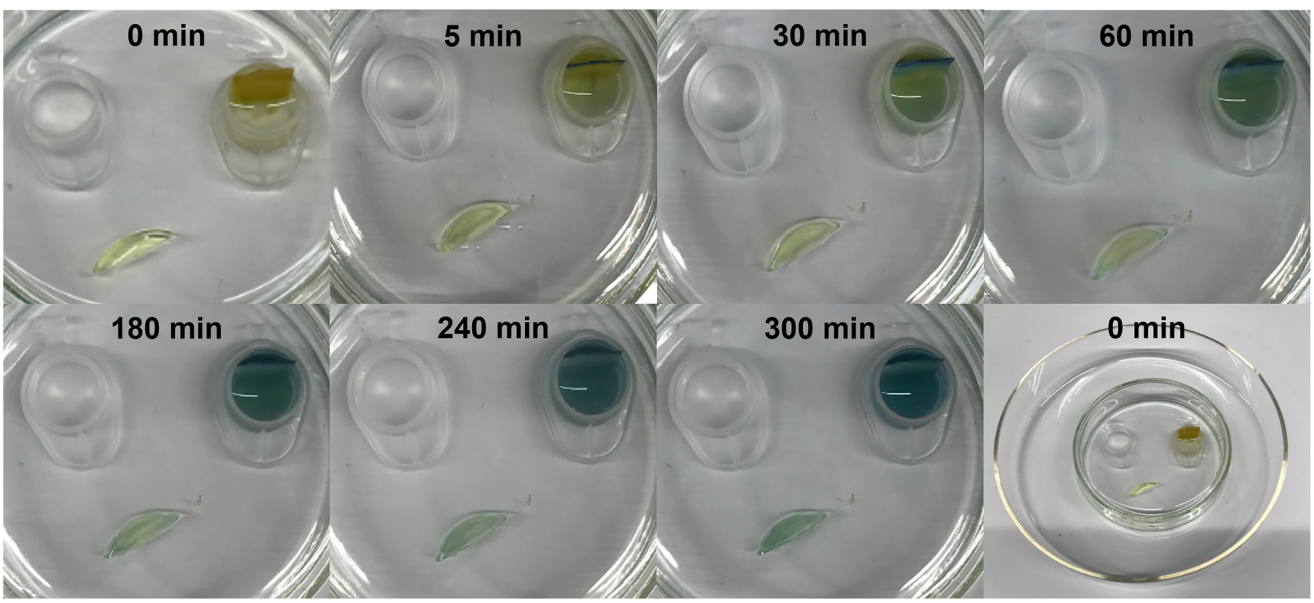

Fig. 6 The BTB-HPC response to the presence of an amine at 40 °C in Milli-Q water for 2 h. The top left reservoir contains 200 μL of aqueous solution of 12 mM methylamine, while the top right reservoirs have small pieces of the pH indicator paper in Milli-Q water. The optical images were taken at the following time points, from left to right: t = 0 min, 5 min, 30 min, 60 min, 180 min, 240 min, and 300 min. Illustration of the setup used to detect the presence of amine at t = 0 min (bottom right, last image).

This journal is © The Royal Society of Chemistry 2025

Open Access Article. Published on 08 May 2025. Downloaded on 1/24/2026 9:10:55 AM.
This article is licensed under a Creative Commons Attribution-NonCommercial 3.0 Unported Licence.

being preserved as long as the hydration is maintained. By combining nanoscale polymersomes with a macroscopic, stimuli-responsive hydrogel matrix, our study presents a novel hybrid sensing platform. Integrated within food packaging as small sachets or pads protected by a thin, semipermeable barrier, HPC-based sensors can effectively detect spoilage-related changes. This approach offers a straightforward and reliable step forward in the application of nanostructured materials for real-time, visible monitoring of food freshness and storage conditions, advancing the development of smart packaging technologies.

Conclusions

By embedding polymersomes loaded with reporting molecules within hydrogels, we successfully created multifunctional HPCs endowed with a temperature-controlled release function, and the capacity to sense small pH changes and visualise the presence of amines, such as those originating from food spoilage. The ability of PDMS-*b*-PMOXA amphiphilic diblock copolymers to encapsulate hydrophilic reporting molecules into their lumen was used as a straightforward approach for generating pH-reporting polymersomes. The entrapment of dye-loaded polymersomes into PNIPAM hydrogels during their synthesis serves not only as a facile pathway to develop stable spatially segregated self-assembled nanostructures with localized functionality, but also as a temperature-responsive polymer network for the stimuli-triggered breakage of polymersomes and release of the encapsulated cargo. The immobilization of polymersomes within the hydrogel matrix preserves their morphology and prevents undesired leakage and contamination of the environment. Carboxyfluorescein-HPCs, when exposed to temperatures above 40 °C, showed a tenfold increase in fluorescence over 24 h compared to carboxyfluorescein-HPCs stored at 25 °C, for which only a very small change in fluorescence was detected during the same time. Furthermore, HPCs encapsulating pyranine were able to detect small pH changes ranging from 6.2 to 8.0, a pH domain suitable for the detection of food spoilage-related analytes. In addition, HPCs loaded with bromothymol blue exhibited a visible colour change from yellow to blue in the presence of 1 mM methylamine, which is 2.5 times lower than the concentration accepted as dangerous for the human body. The combination of pH-reporting polymersomes with temperature-responsive hydrogels results in a versatile chemical sensor for the detection of pH changes caused, for example, by the presence of volatile amines from spoiled food products. Furthermore, our platform enables the release of an encapsulated cargo by exposure to spoilage-related temperatures, when the aim is to detect the occurrence of unsuitable temperatures in the logistics chain with consequences on food quality. Therefore, our HPC system opens new avenues for multifunctional sensing and/or release devices for a broad range of applications including food quality, biomedicine or environmental science.

Author contributions

Conceptualization, project administration and supervision: C. G.P. and I.A.D.; funding acquisition: C.G.P.; investigation and methodology: C.J. and R.P.W.; formal analysis: C.J., E.C.S., R.P. W., and D.M; visualization: C.J. and R.P.W.; writing – original draft: C.J., E.C.S., and I.A.D; writing – review: all authors; and writing – finalization of manuscript: C.J., C.G.P., and I.A.D.

Data availability

The data supporting this article have been included as part of the ESI.†

Conflicts of interest

There are no conflicts to declare.

Acknowledgements

We gratefully acknowledge the financial support of this project by the Swiss National Science Foundation (SNFS) and the University of Basel. Additionally, we gratefully acknowledge Dr M. J. Skowicki (University of Basel) for technical help with confocal laser scanning microscopy experiments and interpretation. We take the opportunity to thank late Prof. Dr Wolfgang P. Meier for his great support and engagement in introducing this study until he passed away in January 2022. We thank Manuel Kraus for the advice on preparing Fig. 1 and the TOC image.

References

1 H. Cheng, H. Xu, D. J. McClements, L. Chen, A. Jiao, Y. Tian, M. Miao and Z. Jin, *Food Chem.*, 2022, **375**, 131738.
2 P. Shao, L. Liu, J. Yu, Y. Lin, H. Gao, H. Chen and P. Sun, *Trends Food Sci. Technol.*, 2021, **118**, 285–296.
3 H. Yousefi, H.-M. Su, S. M. Imani, K. Alkhaldi, C. D. M. Filipe and T. F. Didar, *ACS Sens.*, 2019, **4**, 808–821.
4 C. Ruiz-Capillas and A. M. Herrero, *Foods*, 2019, **8**, 62.
5 I. Craciun, A. S. Denes, G. Gunkel-Grabole, A. Belluati and C. G. Palivan, *Helv. Chim. Acta*, 2018, **101**, e1700290.
6 X. Wan, Q. He, X. Wang, M. Liu, S. Lin, R. Shi, J. Tian and G. Chen, *Food Control*, 2021, **130**, 108355.
7 H. Niu, M. Zhang, D. Shen, A. S. Mujumdar and Y. Ma, *Crit. Rev. Food Sci. Nutr.*, 2023, **64**, 8114–8132.
8 T. H. Wu and P. J. Bechtel, *J. Aquat. Food Prod. Technol.*, 2008, **17**, 27–38.
9 R. Jia, W. Tian, H. Bai, J. Zhang, S. Wang and J. Zhang, *Nat. Commun.*, 2019, **10**, 795.
10 X. Zhai, Y. Xue, W. Song, Y. Sun, T. Shen, X. Zhang, Y. Li, D. Zhang, C. Zhou, J. Zhang, M. Arslan, H. E. Tahir, Z. Li,

Open Access Article. Published on 08 May 2025. Downloaded on 1/24/2026 9:10:55 AM. This article is licensed under a Creative Commons Attribution-NonCommercial 3.0 Unported Licence.

J. Shi, X. Huang, X. Zou, M. Holmes and M. J. Povey, *J. Agric. Food Chem.*, 2024, **72**, 21854–21868.
11 C. Zhou, D.-W. Sun, J. Ma, A. Qin, B. Z. Tang, X.-R. Lin and S.-L. Cao, *ACS Appl. Mater. Interfaces*, 2024, **16**, 6533–6547.
12 M. Nami, M. Taheri, J. Siddiqui, I. A. Deen, M. Packirisamy and M. Jamal Deen, *Adv. Mater. Technol.*, 2024, **9**, 2301347.
13 M. J. Grant, K. M. Wolfe, C. R. Harding and G. C. Welch, *J. Mater. Chem. C*, 2023, **11**, 9749.
14 I. M. Karaca, G. Haskaraca, Z. Ayhan and E. Gültekin, *Food Res. Int.*, 2023, **173**, 113261.
15 X. Luo, A. Zaitoon and L.-T. Lim, *Compr. Rev. Food Sci. Food Saf.*, 2022, **21**, 2489–2519.
16 A. I. Danchuk, N. S. Komova, S. N. Mobarez, S. Y. Doronin, N. A. Burmistrova, A. V. Markin and A. Duerkop, *Anal. Bioanal. Chem.*, 2020, **412**, 4023–4036.
17 B. Kuswandi and A. Nurfawaidi, *Food Control*, 2017, **82**, 91–100.
18 C. Schaude, C. Meindl, E. Frohlich, J. Attard and G. J. Mohr, *Talanta*, 2017, **170**, 481–487.
19 C. Calvino, M. Piechowicz, S. J. Rowan, S. Schrettl and C. Weder, *Chem. – Eur. J.*, 2018, **24**, 7369–7373.
20 X. Yang, C. Jin, J. Zheng, F. Chai and M. Tian, *Sens. Actuators, B*, 2023, **394**, 134417.
21 A. O. Santos, A. Vaz, P. Rodrigues, A. C. A. Veloso, A. Venâncio and A. M. Peres, *Chemosensors*, 2019, **7**, 3.
22 Y.-J. Jin and G. Kwak, *Sens. Actuators, B*, 2018, **271**, 183–188.
23 Y. Takagai, Y. Nojiri, T. Takase, W. L. Hinze, M. Butsugan and S. Igarashi, *Analyst*, 2010, **135**, 1417–1425.
24 P. R. Lakshmi, B. Mohan, P. Kang, P. Nanjan and S. Shanmugaraju, *Chem. Commun.*, 2023, **59**, 1728–1743.
25 F. Behoftadeh, M. F. Ghasemi, A. Mojtahedi, K. Issazadeh, M. Golshekan and S. Alaei, *Arch. Microbiol.*, 2023, **205**, 70.
26 D. Kong, R. Jin, T. Wang, H. Li, X. Yan, D. Su, C. Wang, F. Liu, P. Sun, X. Liu, Y. Gao, J. Ma, X. Liang and G. Lu, *Biosens. Bioelectron.*, 2019, **145**, 111706.
27 X. Zhong, D. Huo, H. Fa, X. Luo, Y. Wang, Y. Zhao and C. Hou, *Sens. Actuators, B*, 2018, **274**, 464–471.
28 F. Mustafa and S. Andreescu, *Foods*, 2018, **7**, 168.
29 K. Völlmecke, R. Afroz, S. Bierbach, L. J. Brenker, S. Frücht, A. Glass, R. Giebelhaus, A. Hoppe, K. Kanemaru, M. Lazarek, L. Rabbe, L. Song, A. Velasco Suarez, S. Wu, M. Serpe and D. Kuckling, *Gels*, 2022, **8**, 768.
30 W. Cheng, X. Wu, Y. Zhang, D. Wu, L. Meng, Y. Chen and X. Tang, *Trends Food Sci. Technol.*, 2022, **129**, 244–257.
31 M. Garni, R. Wehr, S. Y. Avsar, C. John, C. Palivan and W. Meier, *Eur. Polym. J.*, 2019, **112**, 346–364.
32 E. Rideau, R. Dimova, P. Schwille, F. R. Wurm and K. Landfester, *Chem. Soc. Rev.*, 2018, **47**, 8572–8610.
33 O. Onaca, R. Enea, D. W. Hughes and W. Meier, *Macromol. Biosci.*, 2009, **9**, 129–139.
34 A. Moquin, J. Ji, K. Neibert, F. M. Winnik and D. Maysinger, *ACS Omega*, 2018, **3**, 13882–13893.
35 M. V. Dinu, I. A. Dinu, S. S. Saxer, W. Meier, U. Pieles and N. Bruns, *Biomacromolecules*, 2021, **22**, 134–145.
36 D. Gräfe, J. Gaitzsch, D. Appelhans and B. Voit, *Nanoscale*, 2014, **6**, 10752–10761.
37 C. Nehate, A. Nayal and V. Koul, *ACS Biomater. Sci. Eng.*, 2019, **5**, 70–80.
38 L. J. C. Albuquerque, V. Sincari, A. Jäger, J. Kucka, J. Humajova, J. Pankrac, P. Paral, T. Heizer, O. Janouškova, I. Davidovich, Y. Talmon, P. Pouckova, P. Štěpánek, L. Sefc, M. Hruby, F. C. Giacomelli and E. Jäger, *J. Controlled Release*, 2021, **332**, 529–538.
39 M. Lomora, F. Itel, I. A. Dinu and C. G. Palivan, *Phys. Chem. Chem. Phys.*, 2015, **17**, 15538–15546.
40 I. Craciun, G. Gunkel-Grabole, A. Belluati, C. G. Palivan and W. Meier, *Nanomedicine*, 2017, **12**, 811–817.
41 M. Kumar, M. Grzelakowski, J. Zilles, M. Clark and W. Meier, *Proc. Natl. Acad. Sci. U. S. A.*, 2007, **104**, 20719–20724.
42 C. E. Meyer, I. Craciun, C.-A. Schoenenberger, R. Wehr and C. G. Palivan, *Nanoscale*, 2021, **13**, 66–70.
43 L. Heuberger, M. Korpidou, O. M. Eggenberger, M. Kyropoulou and C. G. Palivan, *Int. J. Mol. Sci.*, 2022, **23**, 5718.
44 V. Maffeis, D. Hürlimann, A. Krywko-Cendrowska, C.-A. Schoenenberger, C. E. Housecroft and C. G. Palivan, *Small*, 2023, **19**, 2202818.
45 M. Mahinroosta, Z. Jomeh Farsangi, A. Allahverdi and Z. Shakoori, *Mater. Today Chem.*, 2018, **8**, 42–55.
46 J. Li and D. J. Mooney, *Nat. Rev. Mater.*, 2016, **1**, 16071.
47 S. J. Buwalda, T. Vermonden and W. E. Hennink, *Biomacromolecules*, 2017, **18**, 316–330.
48 B. V. K. J. Schmidt, *Macromol. Rapid Commun.*, 2022, **43**, 2100895.
49 Y. Hong, Y. Xi, J. Zhang, D. Wang, H. Zhang, N. Yan, S. He and J. Du, *J. Mater. Chem. B*, 2018, **6**, 6311–6321.
50 M. Babaei, J. Davoodi, R. Dehghan, M. Zahiri, K. Abnous, S. M. Taghdisi, M. Ramezani and M. Alibolandi, *J. Drug Delivery Sci. Technol.*, 2020, **59**, 101885.
51 L. Gao, Z. Yuan, N. Ma, X. Zhou, X. Huang, W. Chen and H. Qiao, *Chem. Eng. J.*, 2024, **485**, 149688.
52 S. L. Banerjee, S. Samanta, S. Sarkar and N. K. Singha, *J. Mater. Chem. B*, 2020, **8**, 226–243.
53 S. Litvinchuk, Z. Lu, P. Rigler, T. D. Hirt and W. Meier, *Pharm. Res.*, 2009, **26**, 1711–1717.
54 J.-T. Zhang, S.-X. Cheng, S.-W. Huang and R.-X. Zhuo, *Macromol. Rapid Commun.*, 2003, **24**, 447–451.
55 E. Vallés, D. Durando, I. Katime, E. Mendizábal and J. E. Puig, *Polym. Bull.*, 2000, **44**, 109–114.
56 D. Daubian, J. Gaitzsch and W. Meier, *Polym. Chem.*, 2020, **11**, 1237–1248.
57 A. Kumar, A. Srivastava, I. Y. Galaev and B. Mattiasson, *Prog. Polym. Sci.*, 2007, **32**, 1205–1237.
58 G. Yaşayan, M. Redhead, J. P. Magnusson, S. G. Spain, S. Allen, M. Davies, C. Alexander and F. Fernández-Trillo, *Polym. Chem.*, 2012, **3**, 2596–2604.
59 K. Kiene, S. H. Schenk, F. Porta, A. Ernst, D. Witzigmann, P. Grossen and J. Huwyler, *Eur. J. Pharm. Biopharm.*, 2017, **119**, 322–332.

This journal is © The Royal Society of Chemistry 2025

Open Access Article. Published on 08 May 2025. Downloaded on 1/24/2026 9:10:55 AM.
This article is licensed under a Creative Commons Attribution-NonCommercial 3.0 Unported Licence.

60 C. E. Meyer, C.-A. Schoenenberger, R. P. Wehr, D. Wu and C. G. Palivan, *Macromol. Biosci.*, 2021, **21**, 2100249.
61 A. Guinart, M. Korpidou, D. Doellerer, G. Pacella, M. C. A. Stuart, I. A. Dinu, G. Portale, C. Palivan and B. L. Feringa, *Proc. Natl. Acad. Sci. U. S. A.*, 2023, **120**, e2301279120.
62 N. R. Clement and J. M. Gould, *Biochemistry*, 1981, **20**, 1534–1538.
63 W. B. Deichmann and H. W. Gerarde, in *Toxicology of drugs and chemicals*, ed. W. B. Deichmann and H. W. Gerarde, Academic Press, New York, 1969, p. 385.
64 *Patty's industrial hygiene and toxicology: Volume 2B: Toxicology*, ed. D. Clayton and F. E. Clayton, John Wiley & Sons, New York, NY, 1981.
65 T. De Meyer, K. Hemelsoet, V. Van Speybroeck and K. De Clerck, *Dyes Pigm.*, 2014, **102**, 241–250.